LETTERS

Graphene-based composite materials

Sasha Stankovich[1]*, Dmitriy A. Dikin[1]*, Geoffrey H. B. Dommett[1], Kevin M. Kohlhaas[1], Eric J. Zimney[1], Eric A. Stach[3], Richard D. Piner[1], SonBinh T. Nguyen[2] & Rodney S. Ruoff[1]

Graphene sheets—one-atom-thick two-dimensional layers of sp^2-bonded carbon—are predicted to have a range of unusual properties. Their thermal conductivity and mechanical stiffness may rival the remarkable in-plane values for graphite ($\sim$3,000 W m^{-1} K^{-1} and 1,060 GPa, respectively); their fracture strength should be comparable to that of carbon nanotubes for similar types of defects[1–3]; and recent studies have shown that individual graphene sheets have extraordinary electronic transport properties[4–8]. One possible route to harnessing these properties for applications would be to incorporate graphene sheets in a composite material. The manufacturing of such composites requires not only that graphene sheets be produced on a sufficient scale but that they also be incorporated, and homogeneously distributed, into various matrices. Graphite, inexpensive and available in large quantity, unfortunately does not readily exfoliate to yield individual graphene sheets. Here we present a general approach for the preparation of graphene-polymer composites via complete exfoliation of graphite[9] and molecular-level dispersion of individual, chemically modified graphene sheets within polymer hosts. A polystyrene–graphene composite formed by this route exhibits a percolation threshold[10] of $\sim$0.1 volume per cent for room-temperature electrical conductivity, the lowest reported value for any carbon-based composite except for those involving carbon nanotubes[11]; at only 1 volume per cent, this composite has a conductivity of $\sim$0.1 S m^{-1}, sufficient for many electrical applications[12]. Our bottom-up chemical approach of tuning the graphene sheet properties provides a path to a broad new class of graphene-based materials and their use in a variety of applications.

Graphite oxide is a layered material produced by the oxidation of graphite (Fig. 1a). In contrast to pristine graphite, the graphene-derived sheets in graphite oxide (graphene oxide sheets) are heavily oxygenated, bearing hydroxyl and epoxide functional groups on their basal planes, in addition to carbonyl and carboxyl groups located at the sheet edges[13,14]. The presence of these functional groups makes graphene oxide sheets strongly hydrophilic, which allows graphite oxide to readily swell and disperse in water[2,15,16]. Previous studies by our team have shown that a mild ultrasonic treatment of graphite oxide in water results in its exfoliation to form stable aqueous dispersions that consist almost entirely of 1-nm-thick sheets (Fig. 1b)[9]. Given the uniformity of the observed thicknesses and that platelets one-half of the observed minimum thickness are never detected (or any other inverse integer value, such as one-third, and so on), we believe that these represent fully exfoliated graphene oxide sheets. In fact, at present, exfoliation of graphite oxide is the only way to produce stable suspensions of quasi-two-dimensional carbon sheets, making this a strategic starting point for large-scale synthesis of graphene sheets. As such, graphite oxide has recently attracted attention as a filler for polymer nanocomposites[17–19].

Nanocomposites have been heralded[20] as a 'radical alternative to conventional filled polymers or polymer blends,' especially in the fields of transportation and electronics. Unfortunately, owing to their hydrophilic nature, graphene oxide sheets can only be dispersed in aqueous media that are incompatible with most organic polymers. In addition, graphite oxide is electrically insulating, unlike graphite, which limits its usefulness for the synthesis of conductive nanocomposites. It has been demonstrated[9,18,21,22], however, that the electrical conductivity of graphite oxide can be significantly increased by chemical reduction, presumably owing to the restoration of a graphitic network of sp^2 bonds. But reduction of exfoliated graphene oxide nanoplatelets in water results in their irreversible coagulation[9], which then makes dispersion within a polymer matrix at the individual sheet level impossible.

We recently demonstrated that the exfoliation behaviour of graphite oxide can be altered by changing the surface properties of graphene oxide sheets by way of chemical functionalization. A number of chemically modified graphite oxides were prepared by treating graphite oxide with organic isocyanates[23]. The isocyanate treatment reduces the hydrophilic character of graphene oxide sheets by forming amide and carbamate ester bonds to the carboxyl and hydroxyl groups of graphite oxide, respectively. As a result, such isocyanate-derivatized graphite oxides no longer exfoliate in water but readily form stable dispersions in polar aprotic solvents (such as N,N-dimethylformamide (DMF)), consisting of completely exfoliated, functionalized individual graphene oxide sheets with thickness $\sim$1 nm, as determined by atomic force microscopy, AFM (Fig. 1c). These dispersions of isocyanate-derivatized graphite oxide allow graphene oxide sheets to be intimately mixed with many organic polymers, facilitating synthesis of graphene–polymer composites. Coupled with the possibility that graphite oxide can be chemically reduced (see above), we were hopeful that nanocomposites of polymer and isocyanate-derivatized graphite oxide could be rendered electrically conductive.

Hence, we were gratified to find that electrically conductive graphene–polymer nanocomposites can be prepared by solution-phase mixing of the exfoliated phenyl isocyanate-treated graphite oxide sheets with polystyrene, followed by their chemical reduction (Fig. 1d). These composites feature individual graphene sheets well dispersed throughout the polymer matrix (Fig. 1g). Similar dispersions have been achieved with other styrenic polymers such as acrylonitrile-butadiene-styrene and styrene-butadiene rubbers. Chemical reduction was essential for inducing electrical conductivity, as composite samples with un-reduced phenyl isocyanate-treated graphite oxide sheets were insulating. In addition, the presence of the polymer in solution during the reduction step was key to preventing the agglomeration of the sheets. As the reduction proceeds, the sheets become coated with the polymer and remain individually dispersed (Fig. 1d). When the reduction step preceded the introduction of the polymer, significant agglomeration of graphene

[1]Department of Mechanical Engineering, [2]Department of Chemistry, Northwestern University, 2145 Sheridan Road, Evanston, Illinois 60208-3111, USA. [3]School of Materials Engineering and Birck Nanotechnology Center, Purdue University, 501 Northwestern Avenue, West Lafayette, Indiana 47907, USA.
*These authors contributed equally to this work.

sheets occurred. Further details of the preparation and fabrication of composite samples are described in Methods.

In a concurrent research direction, we explored a rapid thermal expansion of graphite oxide (~1,000 °C under inert gas; R. K. Prud'homme *et al.*, manuscript in preparation). However, the thermally expanded graphite oxide platelets so produced are not fully exfoliated, consisting of several-nanometre-thick multilayer stacks, and their dispersion in a polymer matrix is a challenging step of manufacture. For the purpose of comparison, polystyrene composites prepared with such thermally expanded graphite oxide, by the same procedure as was used for phenyl isocyanate-treated graphite oxide, are less homogeneous and have higher electrical percolation thresholds (see Supplementary Information). For this and other reasons, we have focused on the bottom-up approach that yields molecular-level dispersion of individual graphene sheets as observed by scanning electron microscopy, SEM (Fig. 1g).

The quality of nanofiller dispersion in the polymer matrix directly correlates with its effectiveness for improving mechanical, electrical, thermal, impermeability and other properties. The properties of a composite are also intimately linked to the aspect ratio and surface-to-volume ratio of the filler. The potential properties of our graphene-

sheet-based composites thus appear promising owing to the extremely high aspect ratios of the sheets as determined from SEM images (Fig. 1g), in which the average lateral dimension was estimated to be ~1 μm, similar to the values found by AFM (Fig. 1b, c). However, in contrast to the typically flat sheets seen by AFM when deposited onto atomically flat substrates, the sheets in the composites are crumpled and wrinkled, and at times folded.

At 2.4 volume per cent (vol.%) loading, the composite appears in the SEM images to be almost entirely filled with the graphene sheets, even though 97.6 vol.% is still filled by the polymer (Fig. 1g, right panel). This 'visual' effect is due to the enormous surface area of the sheets. The specific surface area of an individual graphene sheet is ~2,600 $m^2 g^{-1}$, so 1 $μm^3$ of a composite with 1 vol.% graphene sheets would have ~50 $μm^2$ of sheet surface area. SEM image analysis was used to estimate the apparent graphene sheet surface area at different concentrations (Fig. 2a–d). It revealed a surface area lower by roughly a factor of two than the calculated values for each concentration. The nanoscale corrugation of the graphene sheets (not evident in SEM imaging) may contribute to the discrepancy. The intrinsic mechanics of the sheets, their crumpling, wrinkling and folding, and whether they can be processed to be non-crumpled (for example, so that
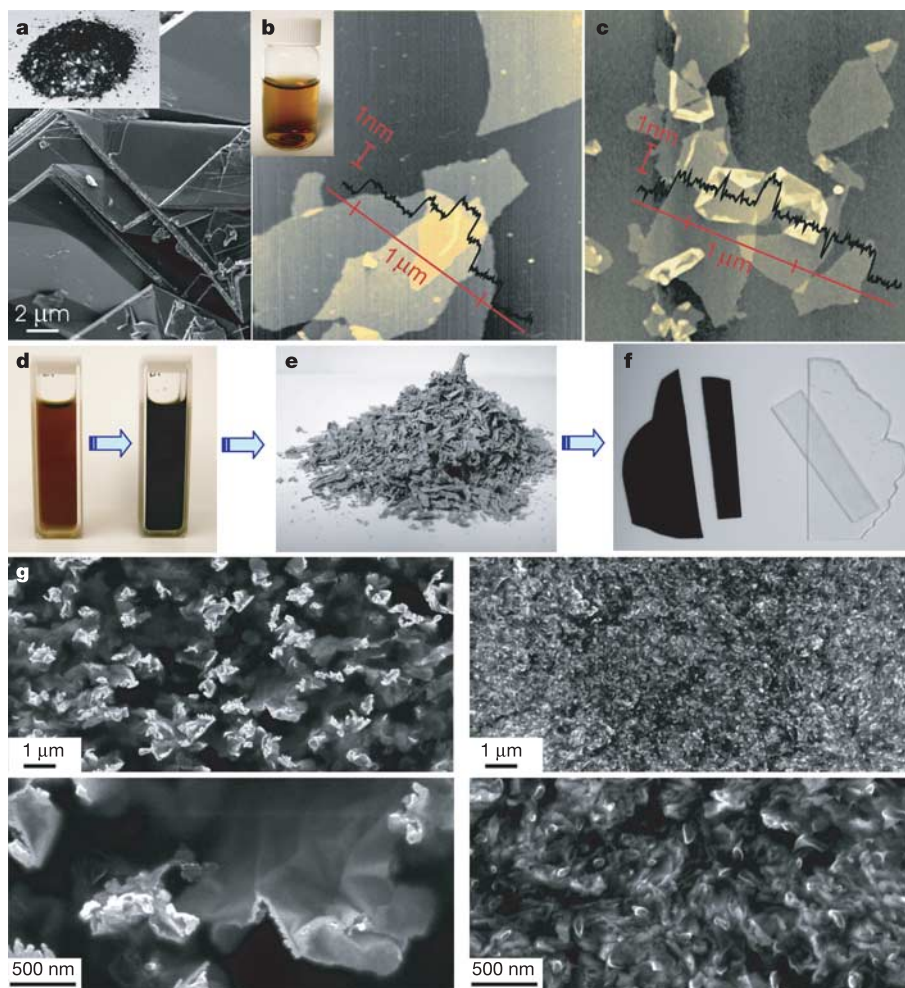
Figure 1 | Process flow of graphene–polymer composite fabrication.
a, SEM and digital image (inset) of natural graphite. **b**, A typical AFM non-contact-mode image of graphite oxide sheets deposited onto a mica substrate from an aqueous dispersion (inset) with superimposed cross-section measurements taken along the red line indicating a sheet thickness of ~1 nm. **c**, AFM image of phenyl isocyanate-treated graphite oxide sheets on mica and profile plot showing the ~1 nm thickness. **d**, Suspension of phenyl isocyanate-treated graphite oxide (1 mg ml^{-1}) and dissolved polystyrene in

DMF before (left) and after (right) reduction by *N*,*N*-dimethylhydrazine.
e, Composite powder as obtained after coagulation in methanol.
f, Hot-pressed composite (0.12 vol.% of graphene) and pure polystyrene of the same 0.4-mm thickness and processed in the same way. **g**, Low (top row) and high (bottom row) magnification SEM images obtained from a fracture surface of composite samples of 0.48 vol.% (left) and 2.4 vol.% (right) graphene in polystyrene.

layering could be more effectively achieved) are issues for further study. Heat treatment of such composites to 300 °C, well above the glass transition temperature of polystyrene (100 °C), does not result in agglomeration of the graphene sheets (as assessed from extensive SEM imaging), suggesting their thermal stability over a broad temperature range.

As SEM cannot spatially resolve the thickness of an individual graphene-based sheet, transmission electron microscopy (TEM) was used to determine if the graphene-based sheets were indeed present in the composites as single, exfoliated sheets or as multi-layered platelets. Extensive high-resolution phase-contrast imaging showed no evidence of multi-layer stacks, even though SEM of the same slices clearly indicated the presence of nanoplatelets. In contrast, selected-area electron diffraction (SAED) of composite samples yielded spot patterns matching those expected for individual graphene-based sheets (Fig. 2e, f, and Supplementary Information). SAED of pure polystyrene samples fabricated in an identical manner (see Methods) showed the ring pattern expected for an amorphous material.

The conductive nature of the graphene filler motivated our study of the percolation behaviour through electrical measurements. As a control, we prepared polystyrene composites containing phenyl isocyanate-treated graphite oxide sheets that were not chemically reduced. At similar graphene concentrations, these samples were greyish in colour compared to the almost black composites filled with the reduced material, and they were not electrically conductive.

To obtain the true value of the conductivity of the composites, we made separate measurements of in-plane and transverse resistances
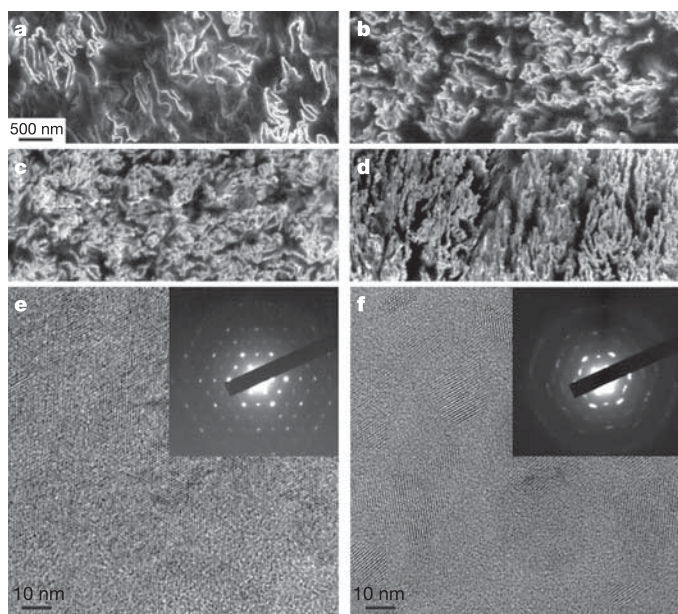

Figure 2 | SEM and TEM images of graphene–polystyrene composite.
a–d, SEM images of the microtomed composites reveal different morphologies of the graphene sheets, including their packing, at different concentrations (vol.%): **a**, 0.24; **b**, 0.96; **c**, 1.44; and **d**, 2.4. Scale bar, shown in **a**, applies to **a–d**. **e**, **f**, High-resolution phase contrast images and SAED patterns (inset) of **e**, cast film made from powder composite, and **f**, microtomed composite sample. The SAED patterns show the six-fold rotational symmetry expected for diffraction with the beam incident along [0001]. Our experimentally obtained patterns show all of the reflections expected for such single graphene-based sheets. The *d* spacings associated with the spots were determined using both gold and graphite calibrants, and the first five sets of spots correspond to *d*-spacings (Å) of 4.23, 2.45, 2.12, 1.42 and 1.23. More details are presented in Supplementary Information. Additionally, these high-resolution images show regions where fringes are observed and regions where they are not, which indicates that there is significant local curvature in the sheets.

(Fig. 3, inset) and developed a numerical simulation program based on FEMLAB (version 3.1, Comsol AB), which takes into account geometry of the samples and electrical leads. All measurements and subsequent analysis revealed minor anisotropy, with the in-plane conductivity, $\sigma_\parallel$, always slightly higher than the transverse conductivity, $\sigma_\perp$.

A rapid increase in the direct current electrical conductivity of composite materials takes place when the conductive filler forms an infinite network of connected paths through the insulating matrix. When the filler particles are rigid bodies, the conductivity of such media is typically described with a bond percolation model[10]. The conductivity of the composite, σ_c, above the percolation threshold is then treated with a power law: $\sigma_c = \sigma_f[(\phi - \phi_c)/(1 - \phi_c)]^t$ (ref. 24), where σ_f is the conductivity of the filler, ϕ the filler volume fraction, ϕ_c the percolation threshold (the onset of the transition), and t is the 'universal critical exponent'.

Percolation in polystyrene–graphene composites occurs when the filler concentration, ϕ_c, is near 0.1 vol.% (Fig. 3). This percolation threshold is, to the best of our knowledge, about three times lower than reported for any other two-dimensional filler[25]. Such a low percolation threshold for a three-dimensional isotropic case is evidently due to the extremely high aspect ratio of the graphene sheets and their excellent homogeneous dispersion in these composites. Randomly oriented oblate ellipsoids (disks) with an aspect ratio of 1,000 are predicted to have a geometric percolation threshold of ~0.1 vol.% (ref. 26). At a loading of about 0.15 vol.%, the conductivity of our composites already satisfies the antistatic criterion (10^{-6} S m^{-1}) for thin films[12] and rapidly rises over a 0.4 vol.% range. An increase in graphene sheet loading above 0.5 vol.% yields a more gradual increase in electrical conductivity, with values of ~0.1 S m^{-1} at 1 vol.% and ~1 S m^{-1} at 2.5 vol.%.

At present, research in nanocomposite materials using carbon-based nanofillers is dominated by carbon nanotubes. The electrical properties of our composites compare well with the best values reported in the literature for nanotube–polymer composites. The
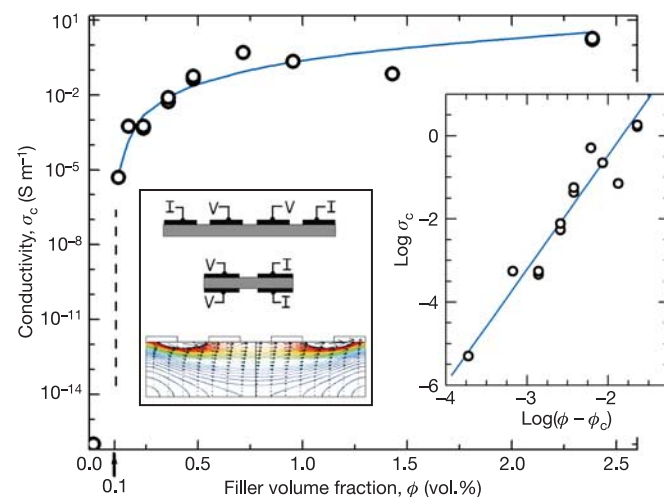
Figure 3 | Electrical conductivity of the polystyrene–graphene composites as a function of filler volume fraction. Main figure, composite conductivity, σ_c, plotted against filler volume fraction, ϕ. Right inset, logσ_c plotted against log($\phi - \phi_c$), where ϕ_c is the percolation threshold (see text). Solid lines in both graphs are calculated conductivities based on the fitting (inset, log–log plot) of the experimental data to the effective conductivity equation described in the text. Fitted parameters are: $t = 2.74 \pm 0.20$, $\sigma_f = 10^{4.92\pm0.52}$ S m^{-1} and $\phi_c = 0.1$ vol.%. Left inset: top and middle diagrams show the four-probe setup for in-plane and transverse measurements, respectively; bottom diagram, one of the computed distributions of the current density (contour lines) with local directions and magnitude (shown by arrows) in a specimen for the following conditions— the sample thickness is twice the electrode width and the gap between them, and the in-plane resistivity is 10 times lower than the transverse resistivity.

percolation threshold of around 0.1 vol.% is almost the same as was achieved for single-wall carbon nanotube (SWNT)–polystyrene composites made by latex technology[27], and just twice and four times higher than those measured for SWNT–polyimide[11,24] and poly(phenyleneethynylene)-functionalized SWNT–polystyrene composites[28], respectively. Absolute conductivities of our graphene–polystyrene composites are also essentially the same as the values reported for SWNT-filled polystyrene composites[27]. However, in contrast to these reports, which feature thin film composites, our samples are made by a quasi-industrial method (hot-pressing; we have also made samples by injection moulding that show similar values of electrical conductivity). Furthermore, graphene sheets have higher surface-to-volume ratios than SWNTs owing to the inaccessibility of the inner nanotube surface to polymer molecules. This makes graphene sheets potentially more favourable for altering all matrix properties—such as the mechanical, rheological and permeability properties, and degradation stability. Also, SWNTs are still much more expensive than graphite, which is a commodity material with about 1,000,000 t used annually, and which is sold for a few US dollars per kilogram[29]. In contrast, graphite oxide can be readily prepared from a vast array of graphites, and its industrial production has also recently become a topic of interest[30].

We therefore expect that our method for preparation and incorporation of individual graphene sheets into polymer matrices will lead to the further development of a broad new class of materials with enhanced properties and even introduce new functionalities to polymer composites.

METHODS

Fabrication of composites. Graphite oxide was prepared by the Hummers method from SP-1 graphite (Bay Carbon), and dried for a week over phosphorus pentoxide in a vacuum desiccator. Dried graphite oxide (50 mg) was suspended in anhydrous DMF (5 ml, Dow-Grubbs solvent system), treated with phenyl isocyanate (2 mmol, Sigma-Aldrich) for 24 h, and recovered by filtration through a sintered glass funnel (50 ml, medium porosity). Stable dispersions of the resulting phenyl isocyanate-treated graphite oxide materials were prepared by ultrasonic exfoliation (Fisher Scientific FS60, 150 W, 1 h) in DMF (1 mg ml^{-1}). Polystyrene (Scientific Polymer Products, approximate M_w = 280 kD, PDI = 3.0) was added to these dispersions and dissolved with stirring (Fig. 1d, left). Reduction of the dispersed material (Fig. 1d, right) was carried out with dimethylhydrazine (0.1 ml in 10 ml of DMF, Sigma-Aldrich) at 80 °C for 24 h. Upon completion, the coagulation of the polymer composites was accomplished by adding the DMF solutions dropwise into a large volume of vigorously stirred methanol (10:1 with respect to the volume of DMF used). The coagulated composite powder (Fig. 1e) was isolated via filtration; washed with methanol (200 ml); dried at 130 °C under vacuum for ~10 h to remove residual solvent, anti-solvent, and moisture; crushed into a fine powder with a mortar and pestle, and then pressed (Fig. 1f) in a hydraulic hot press (Model 0230C-X1, PHI-Tulip) at 18 kN with a temperature of 210 °C. Further description of the composite samples' preparation is given in Supplementary Information. To convert wt% loading of graphene sheets in the composite samples to vol.% (as used in the text), a density for the phenyl isocyanate-treated graphite oxide sheets of 2.2 g cm^{-3} was assumed along with the known density of polystyrene, 1.05 g cm^{-3}. Composites of acrylonitrile-butadiene-styrene and styrene-butadiene rubbers (Sigma-Aldrich) were similarly prepared using the appropriate copolymers.

Microscopy. AFM images were taken on an AutoProbe CP/MT scanning probe microscope (MultiTask; Veeco Instruments). Imaging was done in non-contact mode using a V-shaped 'Ultralever' probe B (Park Scientific Instruments, boron-doped Si with frequency f_c = 78.6 kHz, spring constants k = 2.0–3.8 N m^{-1}, and nominal tip radius 10 nm). All images were collected under ambient conditions at 50% relative humidity and 23 °C with a scanning raster rate of 1 Hz. Samples for AFM images were prepared by depositing dispersions of functionalized graphite oxide in DMF on a freshly cleaved mica surface (Ted Pella Inc.) and allowing them to dry in air.

Electron micrographs were acquired using a field emission SEM (LEO 1525) and a TEM (JEM-3010, JEOL, operated at 300 kV). Two SEM imaging conditions were used: 'surface imaging' operating at ≤1 kV, and 'sub-surface imaging' at ≥5 kV. Microtomed and cast film samples were prepared for TEM. Pressed composites were microtomed to slices of 40–60 nm thickness (Leica Ultracut UCT, Reichert Inc.) and dropped onto standard TEM grids.

Samples investigated in this way were 0.24, 1.44 and 2.4 vol.%. A polystyrene control sample was also prepared and imaged in this way. Before imaging with TEM, SEM was used to verify that a sufficient amount of highly dispersed platelets were present. Cast-film samples were prepared to image graphene sheets 'lying flat' on the carbon support film, with the beam incident along the [0001] direction of the graphene sheet. A small amount (<0.01 mg) of un-pressed powder composite was dissolved in toluene (10 ml) together with additional polystyrene (<0.02 mg) as diluent. The solution was sonicated (Crest Ultrasonic Tru-Sweep 175HT, 45 W, 1 h) before casting, producing a highly dilute solution that, when cast on a mica substrate, formed a film approximately 40 nm thick, as measured by AFM.

Electrical measurements. Hot-pressed composite samples having 0.3–0.5 mm thickness were cut into strips (1–2 mm wide and 15–20 mm long). A thin 'skin' layer deficient in the phenyl isocyanate-treated graphite oxide platelets was removed by oxygen plasma etching (Plasma-Preen II-862, Plasmatic Systems; 2 torr O$_2$, 1.5 min, 350 W) to reduce the contact resistance between the metal leads and sample tested. After etching, a thin gold film (~25 nm) was thermally deposited (BOC Edwards Auto 306 Evaporation System) on one side of the sample for 'longitudinal' measurements (gap between contacts is 0.15 mm), and on the top and bottom sides for 'transverse' measurements. The d.c. resistance of the composites was measured with a d.c. power supply (HP6612C), digital multimeter (HP34401A) and picoammeter (Keithley 6485) using a standard four-probe technique with a threshold detection limit of 0.1 GΩ.

1. Dresselhaus, M. S. & Dresselhaus, G. Intercalation compounds of graphite. *Adv. Phys.* **51**, 1–186 (2002).
2. Hirata, M., Gotou, T., Horiuchi, S., Fujiwara, M. & Ohba, M. Thin-film particles of graphite oxide 1: High-yield synthesis and flexibility of the particles. *Carbon* **42**, 2929–2937 (2004).
3. Yu, M. F., Lourie, O., Moloni, K., Kelly, T. F. & Ruoff, R. S. Strength and breaking mechanism of multiwalled carbon nanotubes under tensile load. *Science* **287**, 637–640 (2000).
4. Novoselov, K. S. *et al.* Electric field effect in atomically thin carbon films. *Science* **306**, 666–669 (2004).
5. Novoselov, K. S. *et al.* Two-dimensional gas of massless Dirac fermions in graphene. *Nature* **438**, 197–200 (2005).
6. Zhang, Y., Tan, Y.-W., Stormer, H. L. & Kim, P. Experimental observation of the quantum Hall effect and Berry's phase in graphene. *Nature* **438**, 201–204 (2005).
7. Zhang, Y., Small, J. P., Amori, M. E. S. & Kim, P. Electric field modulation of galvanomagnetic properties of mesoscopic graphite. *Phys. Rev. Lett.* **94**, 176803 (2005).
8. Berger, C. *et al.* Ultrathin epitaxial graphite: two-dimensional electron gas properties and a route toward graphene-based nanoelectronics. *J. Phys. Chem. B* **108**, 19912–19916 (2004).
9. Stankovich, S. *et al.* Stable aqueous dispersions of graphitic nanoplatelets via the reduction of exfoliated graphite oxide in the presence of poly(sodium 4-styrenesulfonate). *J. Mater. Chem.* **16**, 155–158 (2006).
10. Stauffer, D. & Aharnoy, A. *Introduction to Percolation Theory* (Taylor & Francis, London, 1991).
11. Ounaies, Z., Park, C., Wise, K. E., Siochi, E. J. & Harrison, J. S. Electrical properties of single wall carbon nanotube reinforced polyimide composites. *Compos. Sci. Technol.* **63**, 1637–1646 (2003).
12. Chung, D. D. L. Electrical applications of carbon materials. *J. Mater. Sci.* **39**, 2645–2661 (2004).
13. He, H., Klinowski, J., Forster, M. & Lerf, A. A new structural model for graphite oxide. *Chem. Phys. Lett.* **287**, 53–56 (1998).
14. Lerf, A., He, H., Forster, M. & Klinowski, J. Structure of graphite oxide revisited. *J. Phys. Chem. B* **102**, 4477–4482 (1998).
15. Hirata, M., Gotou, T. & Ohba, M. Thin-film particles of graphite oxide 2: Preliminary studies for internal micro fabrication of single particle and carbonaceous electronic circuits. *Carbon* **43**, 503–510 (2005).
16. Szabo, T., Szeri, A. & Dekany, I. Composite graphitic nanolayers prepared by self-assembly between finely dispersed graphite oxide and a cationic polymer. *Carbon* **43**, 87–94 (2005).
17. Kovtyukhova, N. I. *et al.* Layer-by-layer assembly of ultrathin composite films from micron-sized graphite oxide sheets and polycations. *Chem. Mater.* **11**, 771–778 (1999).
18. Kotov, N. A., Dekany, I. & Fendler, J. H. Ultrathin graphite oxide-polyelectrolyte composites prepared by self-assembly. Transition between conductive and non-conductive states. *Adv. Mater.* **8**, 637–641 (1996).
19. Cassagneau, T., Guerin, F. & Fendler, J. H. Preparation and characterization of ultrathin films layer-by-layer self-assembled from graphite oxide nanoplatelets and polymers. *Langmuir* **16**, 7318–7324 (2000).
20. Vaia, R. A. & Wagner, H. D. Framework for nanocomposites. *Mater. Today* **7**, 32–37 (2004).
21. Du, X. S., Xiao, M., Meng, Y. Z. & Hay, A. S. Novel synthesis of conductive poly(arylene disulfide)/graphite nanocomposite. *Synth. Met.* **143**, 129–132 (2004).

22. Liu, P. & Gong, K. Synthesis of polyaniline-intercalated graphite oxide by an in situ oxidative polymerization reaction. *Carbon* **37**, 706–707 (1999).
23. Stankovich, S., Piner, R. D., Nguyen, S. T. & Ruoff, R. S. Synthesis and exfoliation of isocyanate-treated graphene oxide nanoplatelets. *Carbon* (in the press).
24. McLachlan, D. S. *et al.* AC and DC percolative conductivity of single wall carbon nanotube polymer composites. *J. Polym. Sci. B* **43**, 3273–3287 (2005).
25. Chen, G., Weng, W., Wu, D. & Wu, C. PMMA/graphite nanosheets composite and its conducting properties. *Eur. Polym. J.* **39**, 2329–2335 (2003).
26. Garboczi, E. J., Snyder, K. A., Douglas, J. F. & Thorpe, M. F. Geometrical percolation threshold of overlapping ellipsoids. *Phys. Rev. E* **52**, 819–828 (1995).
27. Grossiord, N., Loos, J. & Koning, C. E. Strategies for dispersing carbon nanotubes in highly viscous polymers. *J. Mater. Chem.* **15**, 2349–2352 (2005).
28. Ramasubramaniam, R., Chen, J. & Liu, H. Homogeneous carbon nanotube polymer composites for electrical applications. *Appl. Phys. Lett.* **83**, 2928–2930 (2003).
29. Olson, D. W. USGS Mineral Commodity Summaries. ⟨http://minerals.usgs.gov/minerals/pubs/commodity/graphite/graphmcs06.pdf⟩ (2006).
30. Titelman, G. I. & Bron, S. *Method of Manufacturing of Graphite Oxide (GO)* P1391–P1392 (Research Disclosure 500, IMI TAMI Institute for Research & Development Ltd., Haifa, 2005).